# Electronic Supplementary Information

## Strong metal-support interaction in novel core-shell Au-$CeO_2$ nanostructures induced by different pretreatment atmospheres and its influence on CO oxidation

Zhihua Wang, Huifen Fu, Ziwei Tian, Dongmei Han and Fubo Gu*
State Key Laboratory of Chemical Resource Engineering, Beijing University of Chemical Technology, Beijing 100029, China

## 1. Preparation of the templates

### 1.1 Materials

Chloroauric acid ($HAuCl_4$•$3H_2O$) was purchased from Sinopharm (Shanghai, China). Ammonium hydroxide ($NH_3$•$H_2O$, 25 % by weight in water), cerium nitrate and sodium citrate were purchased from Beijing Chemical Works (Beijing, China). Poly(vinyl pyrrolidone) (PVP K30) was purchased from Beijing Yili Fine Chemical Research Institute (Beijing, China). Tetraethylorthosilicate (TEOS) and hexamethylenetetramine (HMTA) were purchased from Xilong Chemical Co., Ltd. (Guangdong, China). All chemicals were analytical-grade reagents.

### 1.2 Preparation of $SiO_2$ NPs

50 mL water was added into a solution of TEOS (2 mL) in ethanol (200 mL) under vigorous stirring at 20 $^oC$. 6 mL $NH_3$•$H_2O$ was added to the above-solution. After 1 h, the products were centrifuged (9000 rpm, 15 min), washed with ethanol and dried in a vacuum oven at 60 $^oC$.

### 1.3 Preparation of $NH_2$-$SiO_2$ NPs

0.5 g $SiO_2$ was dispersed in 50 mL ethanol, and 0.5 mL APTES was added into the solution under vigorous stirring at 30 $^oC$. After 6 h, the products were centrifuged (7000 rpm, 10 min), washed with ethanol and dried in a vacuum oven at 60 $^oC$.

### 1.4 Preparation of $NH_2$-$SiO_2$/Au NPs

Au NPs were prepared according to a previously reported method with slight modification.[1] 5 mL 10 mM $HAuCl_4$•$3H_2O$ (4 g/L) and 190 mL deionized water were added into a three-neck flake at room temperature. 5 mL 10 mM sodium citrate aqueous solution was injected into the above-mentioned solution. Then 3 mL 100 mM $NaBH_4$ aqueous solution was added into the above-solution. The mixture was stirred for 2 h to obtain the Au sol.

1 g $SiO_2$ was dispersed in 50 mL deionized water with the help of ultrasonic wave, and the Au sol was added into the above-solution. After 6 h, the products were centrifuged (4000 rpm, 10 min), washed with ethanol and dried in a vacuum oven at 60 $^oC$.

### 1.5 Preparation of Au@$SiO_2$ NPs

Au NPs were prepared according to a previously reported method with slight modification.[2] In a typical synthesis, 4.5 mL $HAuCl_4$•$3H_2O$ (4 g/L) and 30 mL deionized water were added in a three-neck flake at 100 $^oC$. 1.0 mL sodium citrate aqueous solution (3.0 wt %) was injected quickly into the above-mentioned solution and then refluxed for 30 min. After the solution was cooled down to room temperature, an aqueous solution of PVP K30 (0.03 g/mL, 0.65 mL) was added to the Au sol in order to modify the surfaces of Au NPs to facilitate silica coating. The sol was stirred for 12 h at room temperature. PVP-modified Au NPs were collected by centrifugation (9000 rpm, 30 min) and redispersed in 10 mL deionized water under ultrasonic wave. 5.0 mL PVP-modified Au was added to 20 mL ethanol and vibrated for 2 min in an oscillator. 0.3 mL TEOS and 0.65 mL $NH_3$•$H_2O$ were injected into the above-solution. After 2 h, the products were centrifuged (8000 rpm, 15 min), washed with ethanol and dried in a vacuum oven at 60 $^oC$.

### 1.6 Preparation of H-$CeO_2$ NPs

H-$CeO_2$ NPs were prepared by using $SiO_2$ as templates. 0.1 g $SiO_2$ and 1 g PVP were dispersed in 40 mL deionized water with the help of ultrasonic wave, and the mixture was put in the oil bath at 95 $^oC$. 5 mL 0.5 mmol $Ce(NO_3)_3$ and 5 mL 0.5 mmol HMTA aqueous solutions were added into the above-solution in turn under vigorous stirring. After 2 h, the mixture was cooled down to room temperature, centrifuged (7000 rpm, 10 min) and dried in a vacuum oven at 60 $^oC$ to obtain $SiO_2$@CeOOH. The products were heated from room temperature to 600 $^oC$ with a heating rate of 5 $^oC$/min and kept for 2 h to obtain $SiO_2$@$CeO_2$. Then, the 0.1 g $SiO_2$@$CeO_2$ NPs were dispersed in 40 mL 2 M NaOH aquous solution, and stirred for 24 h. After the products were centrifuged, washed with ethanol and dried in a vacuum oven at 60 $^oC$, the H-$CeO_2$ NPs were obtained.

## 2. Results and discussion

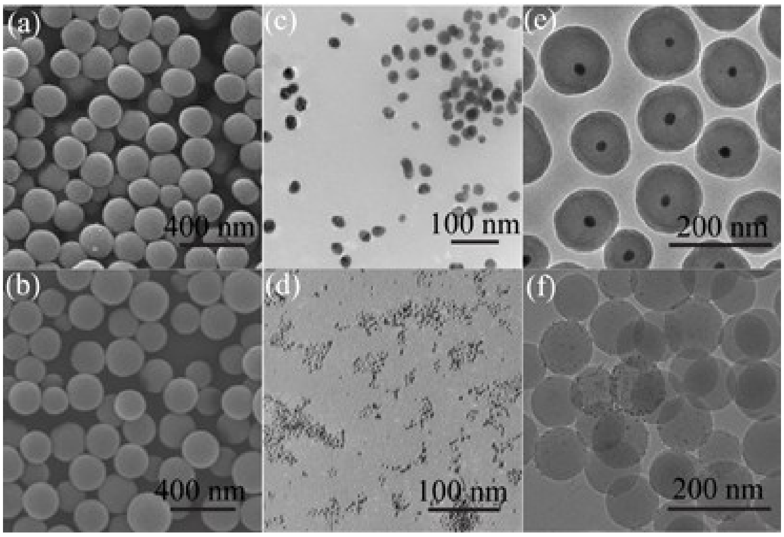

**Fig. S1** SEM images of (a) $SiO_2$ and (b) $NH_2$-$SiO_2$; the TEM images of (c) 25 nm Au NPs, (d) 3-5 nm Au NPs, (e) Au@$SiO_2$ and (f) $NH_2$-$SiO_2$/Au

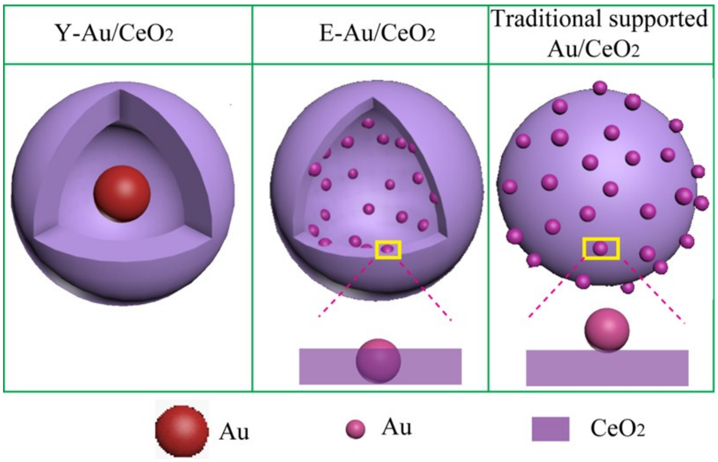

**Scheme S1** Schematic illustration of difference of Y-Au/$CeO_2$, E-Au/$CeO_2$ and traditional supported Au/$CeO_2$.

**Table S1** Recent studies on the Au-based nanocatalysts for CO oxidation

| Catalysts | r* ($mol_{CO}$ $g^{-1}_{Au}$ $h^{-1}$) | Content of Au (*wt*%) | Size of Au (nm) | Ref. |
|---|---|---|---|---|
| Au/$TiO_2$ | 0.72 | 1 | 3.7 | 19 |
| Au/FeOx | 0.61 | 3 | 4.6 | 20 |
| Au/$CeO_2$ | 0.55 | 2.18 | 5 | 21 |
| Au/$Co_3O_4$ | 0.36 | 3 | 3 | 22 |
| Au/$SiO_2$ | 0.27 | 2 | 5 | 23 |
| E-Au/$CeO_2$ | 1.06 | 0.63 | 3-5 | This work |

r*：calculated at 75 °C

**Table S2** The grain sizes of the $CeO_2$ in different catalysts calculated from XRD data

| **Catalysts** | **Y-Au/$CeO_2$-$H_2$** | **Y-Au/$CeO_2$-$O_2$** | **E-Au/$CeO_2$-$H_2$** | **E-Au/$CeO_2$-$O_2$** |
|---|---|---|---|---|
| **Grain sizes (nm) of $CeO_2$** | 10.0 | 9.4 | 10.5 | 9.0 |

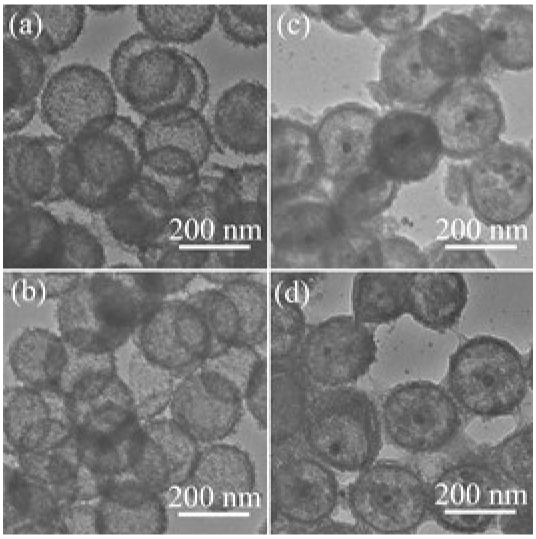

**Fig. S2** TEM images of (a) E-Au/$CeO_2$-$H_2$, (b) E-Au/$CeO_2$-$O_2$, (c) Y-Au/$CeO_2$-$H_2$ and (d) Y-Au/$CeO_2$-$O_2$ after the catalytic reaction

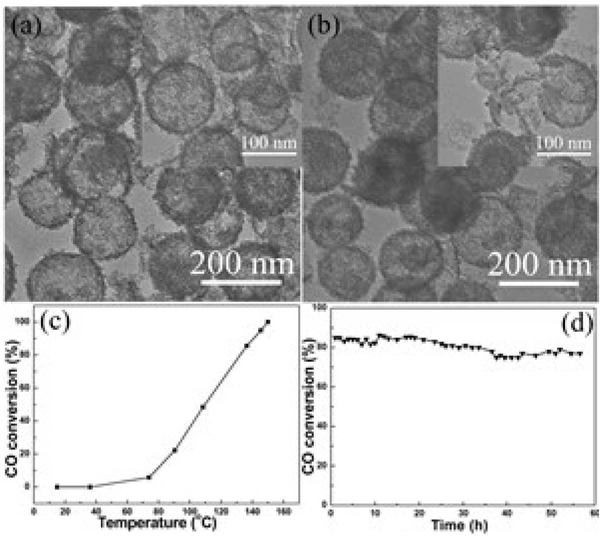

**Fig. S3** TEM images of I-Au/$CeO_2$ NPs: (a) before the catalytic reaction, (b) after the catalytic reaction; (c) conversion curve and (d) stability of I-Au/$CeO_2$ for CO oxidation at 135 °C

## The effect of oxygen vacancy on the activity of H-$CeO_2$

TEM images (Fig. S4a and b) of H-$CeO_2$-$H_2$ and H-$CeO_2$-$O_2$ show that the sizes of these two catalysts are 190 nm, and the thicknesses of the $CeO_2$ shells are 10 nm. The size and shape of the two catalysts are similar. In Fig. S4c, the diffraction peaks can be indexed to be cubic $CeO_2$ (PDF 34-0394). The diffraction peaks widen severely, indicating that the sizes of the crystalline grains of the $CeO_2$ are small (Table S4). The diffraction patterns of the $CeO_2$ are similar for all the samples pretreated in $O_2$ and $H_2$. The specific surface area of H-$CeO_2$ is 226.7 $m^2/g$, and the pore diameters are mainly distributed at about 4 nm (Fig. S4d).

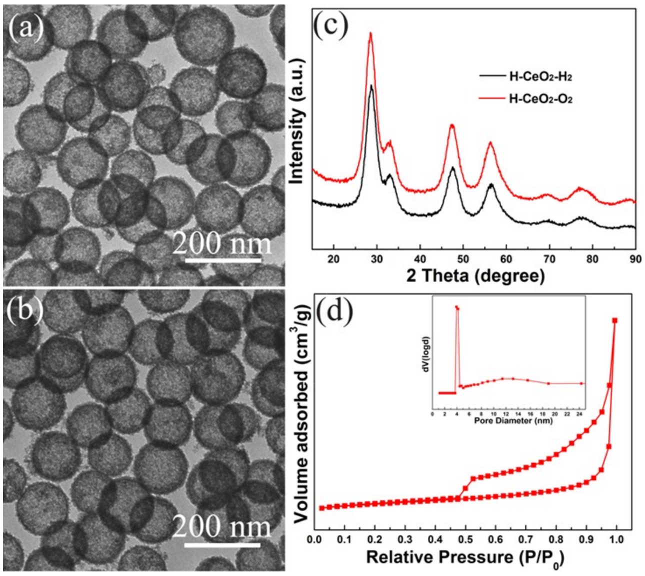

**Fig. S4** TEM images of (a) H-$CeO_2$-$H_2$ and (b) H-$CeO_2$-$O_2$. (c) XRD patterns and (d) Nitrogen adsorption-desorption isotherms, the inset is pore size distributions of H-$CeO_2$.

**Table S3** The grain sizes of the $CeO_2$ in H-$CeO_2$-$H_2$ and H-$CeO_2$-$O_2$ calculated from XRD data.

| **Catalysts** | **H-$CeO_2$-$H_2$** | **H-$CeO_2$-$O_2$** |
|---|---|---|
| **Grain sizes (nm) of $CeO_2$** | 8.5 | 8.4 |

It can be seen that the CO conversion ratio of H-$CeO_2$-$H_2$ is higher than that of H-$CeO_2$-$O_2$ (Fig. S5a). Fig. S5b shows the Ce3d XPS spectra of H-$CeO_2$-$H_2$ and H-$CeO_2$-$O_2$. The peaks at 886 and 905 eV are assigned to $Ce^{3+}$.[3-5] It is clearly seen that the amount of the $Ce^{3+}$ of H-$CeO_2$-$H_2$ is higher than that of H-$CeO_2$-$O_2$, suggesting that the $Ce^{4+}$ is reduced to $Ce^{3+}$ by $H_2$.

As reported in the literature,[6] oxygen vacancy was produced when $Ce^{4+}$ was reduced to $Ce^{3+}$, and the amount of the adsorbed oxygen increased with the increasing of the oxygen vacancy, leading to the enhancement of the catalytic activity.

The O1s results of H-$CeO_2$ are shown in Fig S5c. Taking H-$CeO_2$-$H_2$ for example, three peaks at 530.7, 532.0 and 533.4 eV are obtained This three peaks can be assigned to OI, OII and OIII. The OI belongs to lattice oxygen, OII is associated with the $O^{2-}$ ions in the oxygen deficient regions and OIII is attributed to absorbed oxygen, respectively.[7-10] In Table S4, the relative amount OII for H-$CeO_2$-$H_2$ is higher than that for the H-$CeO_2$-$O_2$, that is, the ruductive atmosphere facilitate the formation of oxygen vacancy.

Visible Raman spectra (514 nm) of H-$CeO_2$ are shown in Fig. S5d, The samples exhibit Raman peak at about 460 $cm^{-1}$, which can be assigned to the F2g vibration mode of the cubic fluorite lattice.[11,12] Defect induced mode (D band) centers at approximately 600 $cm^{-1}$.[13,14] The peak intensity of the D band depends on the amount of oxygen vacancies, and the different relative intensity of D/F2g can illustrated the change of the amount of oxygen vacancy on $CeO_2$.[15-17] It can be seen that the relative amount of oxygen vacancy of the catalysts pretreated in $H_2$ is higher than that of the catalysts pretreated in $O_2$, which correspond to the results obtained from O1s XPS. As reported in the literature, the CO oxidation activity mainly depend on the oxygen vacancy for $CeO_2$.[14,18]

For H-$CeO_2$, the larger relative amount of the oxygen vacancy in H-$CeO_2$-$H_2$ leads to the better activity compared with H-$CeO_2$-$O_2$, revealing that the oxygen vacancy is the main factor to influencing the activity of H-$CeO_2$. So, the activity of H-$CeO_2$-$H_2$ is larger than that of H-$CeO_2$-$O_2$.

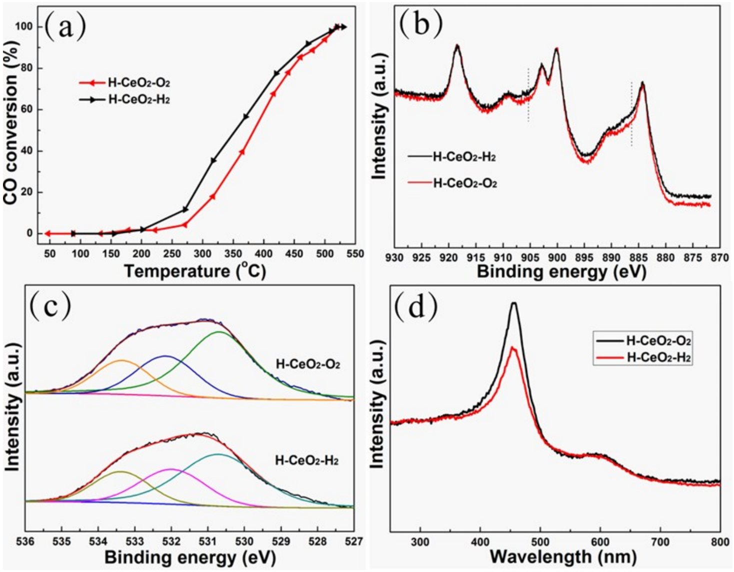

**Fig. S5** (a) Conversion curves for CO oxidation, (b) Ce3d XPS spectra, (c) O1s XPS spectra and (d) Raman spectra of H-$CeO_2$-$H_2$ and H-$CeO_2$-$O_2$.

**Table S4** Comparison of relative amount of oxygen species for H-$CeO_2$-$H_2$

and H-$CeO_2$-$O_2$ obtained from O1s XPS spectra

| Catalysts | H-$CeO_2$-$H_2$ | H-$CeO_2$-$O_2$ |
|---|---|---|
| OI (%) | 54.2 | 57.5 |
| OII (%) | 25.9 | 23.8 |
| OIII (%) | 19.9 | 18.7 |

### The effect of oxygen vacancy on the activities of Y-Au/$CeO_2$ and E-Au/$CeO_2$

In Table S5, the relative amount of the OII for Y-Au/$CeO_2$-$H_2$ is higher than that for Y-Au/$CeO_2$-$O_2$. The relative amount of the OII for E-Au/$CeO_2$-$H_2$ is also higher than that of E-Au/$CeO_2$-$O_2$. The O1s XPS results reveal that the reductive atmosphere facilitate the formation of oxygen vacancy. In Fig. S6b, it can be seen that the relative amounts of oxygen vacancy of the Au/$CeO_2$ pretreated in $H_2$ are higher than those of the catalysts pretreated in $O_2$, which correspond to the results obtained from O1s XPS.

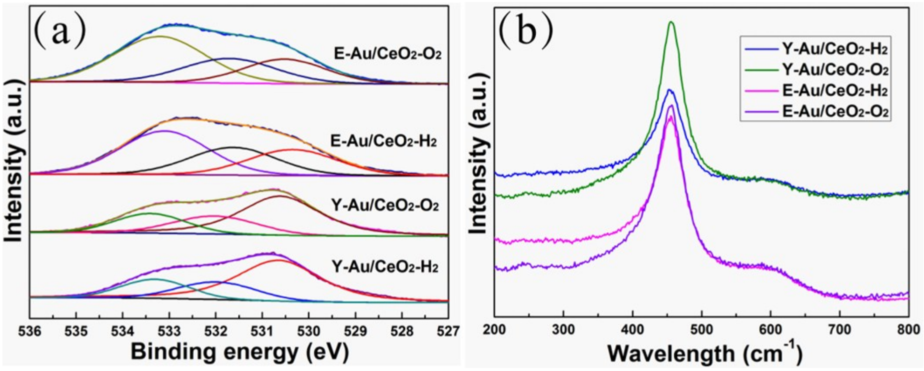

**Fig. S6** (a) O1s XPS and (b) Raman spectra of different catalysts.

**Table S5** Relative amount of oxygen species for different catalysts obtained from O1s XPS spectra

| Catalysts | Y-Au/$CeO_2$-$H_2$ | Y-Au/$CeO_2$-$O_2$ | E-Au/$CeO_2$-$H_2$ | E-Au/$CeO_2$-$O_2$ |
|---|---|---|---|---|
| OI (%) | 61.9 | 61.9 | 27.0 | 23.8 |
| OII (%) | 21.9 | 19.4 | 28.4 | 26.9 |
| OIII (%) | 16.2 | 18.7 | 44.6 | 49.3 |

The CO oxidation activity mainly depends on the oxygen vacancy for H-$CeO_2$. However, the activity of Y-Au/$CeO_2$-$H_2$ is lower than that of Y-Au/$CeO_2$-$O_2$ although the relative amount of the oxygen vacancy for Y-Au/$CeO_2$-$H_2$ is higher than that of Y-Au/$CeO_2$-$O_2$, indicating that the effect of oxygen vacancy on the activity was little for Y-Au/$CeO_2$. The Raman result of E-Au/$CeO_2$ is similar to that of Y-Au/$CeO_2$, that is, the main factor to influencing the activity of Y-Au/$CeO_2$ and E-Au/$CeO_2$ is Au and SMSI between Au and $CeO_2$.

## References

[1] J. Du, J. Qi, D. Wang and Z. Tang, *Energy Environ. Sci.*, 2012, **5**, 6914.

[2] Y. Chen, H. Chen, L. Guo, Q. He, F. Chen, J. Zhou, J. Feng and J. Shi, *ACS Nano*, 2010, **4**, 529.

[3] C. Wen, Y. Zhu, Y. Ye, S. Zhang, F. Cheng, Y. Liu, P. Wang and F. Tao, *ACS Nano*, 2012, **6**, 9305.

[4] S. Zhang, X. Li, B. Chen, X. Zhu, C. Shi and A. Zhu, *ACS Catal.*, 2014, **4**, 3481.

[5] M. Khan, S. Ansari, D. Pradhan, D. Han, J. Lee and M. Cho, *Ind. Eng. Chem. Res.*, 2014, **53**, 9754.

[6] X. Liu, K. Zhou, L. Wang, B. Wang and Y. Li, *J. Am. Chem. Soc.*, 2009, **131**,3140.

[7] M. Chen, Z. Wang, D. Han, F. Gu and G. Guo. Sens. Actuators B, 2011, 157, 565.

[8] M. Chen, Z. Wang, D. Han, F. Gu and G. Guo. *J. Phys. Chem. C*, **2011**, *115*, 12763.

[9] Z. Wang, J. Xue, D. Han and Fubo Gu. *ACS Appl. Mater. Interfaces*, 2015, **7**, 308.

[10] Y. Peng, Y. Wang, Q. G. Chen, Q. Zhu, A. W. Xu. *CrystEngComm*, 2014, **16**, 7906.

[11] Y. Lee, G. He, A. J. Akey, R. Si, M. Flytzani-Stephanopoulos and I. P. Herman. *J. Am. Chem. Soc.*, 2011, **133**, 12952.

[12] W. Lei, T. Zhang, L. Gu, P. Liu, J.´A. Rodriguez, G. Liu and M. Liu. *ACS Catal.*, 2015, **5**, 4385.

[13] Y. Lee, G.He, A. J. Akey, R. Si, Ma. Flytzani-Stephanopoulos and I.P. Herman. *J. Am. Chem. Soc.,* 2011, **133**, 12952.

[14] J. Wang, S. Lin, Z. Han and Y. Liu. *RSC Adv.*, 2015, **5**, 28619.

[15] H. Tan, J. Wang, S. Yu and K. Zhou. *Environ. Sci. Technol.*, 2015, **49**, 8675.

[16] J. Lin, L. Li, Y. Huang, W. Zhang, X. Wang, A. Wang and T. Zhang. *J. Phys. Chem. C*, 2011, **115**, 16509.

[17] P.Pal., R. K. Singha., A. Saha., R. Bal and A. B. Panda. *J. Phys. Chem. C*, 2015, **119**, 13610.

[18] Z. Pu, X. Liu, A. Jia, Y. Xie, J. Lu and M. Luo. *J. Phys. Chem. C*, 2008, **112**, 15045.